

# Simultaneous Inversion for Fast Azimuth and Dispersion of Borehole Flexural Waves Using Cross-Dipole Data

Victoria Briggs, Xiaojun Huang, Rama Rao V.N. and Daniel R. Burns  
Earth Resources Laboratory  
Dept. of Earth, Atmospheric, and Planetary Sciences  
Massachusetts Institute of Technology  
Cambridge, MA 02139

## Abstract

This paper presents an inversion algorithm for obtaining azimuthal angle and borehole flexural wave dispersion in an anisotropic formation. The technique constructs an objective function that can be minimized using standard non-linear inversion methods, which is sensitive to both dispersion and rotation. The method is tested on both synthetic and real borehole data and gives good agreement with traditional processing.

## 1 Introduction

Successful petroleum recovery is directly dependent on an accurate reservoir model. With a greater focus in recent years on residual deposits, it becomes increasingly important that reservoir models reflect the true subsurface structure. Imaging techniques such as seismic surveys, give a good representation of the reservoir but the images become meaningless without the proper velocity constraints used for depth conversion. Further, if the medium imaged has a directionally-dependent velocity, the model must be adjusted accordingly.

Formation anisotropy is typically either intrinsic or induced. Hydrocarbon reservoirs in sedimentary basins can consist of large amounts of shale, which is generally intrinsically anisotropic. Anisotropy can also be stress induced by the borehole, by fractures or due to geologic location.

Besides time to depth conversion, anisotropy measurements can be used to calculate ‘in-situ’ stress fields around the borehole (Huang, 1998) and to determine fracture density and direction (Joyce et al., 1998). Traditionally, anisotropy is estimated from directional borehole measurements which are then corrected before being processed further. Previous work has shown feasibility of a joint inversion of the waveforms for formation shear velocities (without dispersion) and azimuth (Tang and Chunduru, 1999) which combines traditional two-step processing into a one-step inversion. In this paper, we describe a method to invert for the full shear wave dispersion curve as well as the azimuth angle.

First, we describe the recorded waveforms in terms of azimuth and formation parameters, and show how the dispersion can be calculated from the array data. Next, we form the objective function that is to be minimized during the inversion and show the results from synthetic data sets. Finally, we invert data from a real tool in a slightly anisotropic clean sand formation.

## 2 Cross-Dipole Data

In order to estimate anisotropy, a directional measurement is essential. Such a measurement can be performed using a cross-dipole acoustic tool. The tool consists of two pairs of acoustic source transducers orthogonally oriented along the x and y axes (as shown in Figure 1) and 16 pairs of receivers, with 8 pairs oriented along the x axis and 8 pairs along the y axis. This source receiver configuration permits a directional measurement of the formation’s acoustic response. Traditional processing involves two steps: first the waveforms are

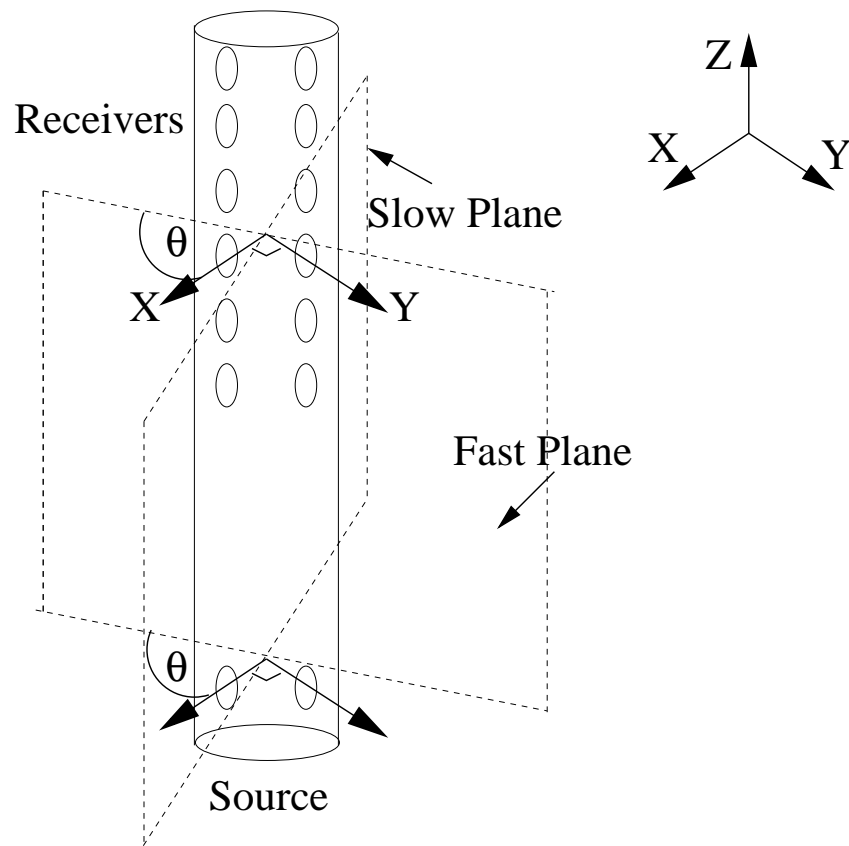


Figure 1: Cross dipole tool.

rotated to calculate the azimuth and to recombine the data into two principal directions (Alford, 1986); second, the two data sets are used individually to estimate the formation shear properties.

When a dipole source is fired in a borehole a set of antisymmetric borehole-guided modes and the relevant refracted waves (shear/compressional) are excited. The guided modes of lowest cut-off frequency, known as flexural modes, are polarized in the x-y plane, perpendicular to their direction of propagation which is along the z-axis. The flexural mode corresponds to the motion of the borehole flexing from side to side in the formation. When the medium is anisotropic the flexural wave motion splits into a fast and a slow component dependent on the directional velocities of the rock and the frequency component of the excitation.

When the source transducer pair oriented along the x-axis is excited, the displacement vector of the flexural wave generated is also in the x direction. The fast and slow axes of the formation make an angle  $\theta$  with respect to the x and y axes so that the displacement vector has projections  $\cos \theta$  and  $\sin \theta$  on the fast and slow directions, respectively. The fast and slow flexural waves then propagate with their respective (frequency dependent) velocities and are recorded at the receivers. Since the receivers are also oriented along the x and y axes, the displacement measured is a second projection of the fast and slow modes back onto the x and y axes. For each receiver offset there are two possible source orientations and two possible receiver orientations, from x-source to x-receiver, inline XX, from x-source to y-receiver, crossline XY, and similarly for the y-source, inline YY and crossline YX.

Let  $S_x(t)$  and  $S_y(t)$  represent the source excitation functions for the x and y oriented dipoles and let  $s_x(\omega)$  and  $s_y(\omega)$  be their fourier transforms. Also let  $g_f^{(n)}(\omega)$  and  $g_s^{(n)}(\omega)$  be the formation propagation function from the source to the  $n^{th}$  receiver, i.e.,

$$g_f^{(n)}(\omega) = \exp\left\{i \frac{\omega}{v_f(\omega)} z_n\right\} \quad (1)$$

$$g_s^{(n)}(\omega) = \exp\left\{i \frac{\omega}{v_s(\omega)} z_n\right\} \quad (2)$$

where  $v_f(\omega)$  and  $v_s(\omega)$  are the fast and slow frequency dependent phase velocities, respectively, and  $z_n$  is the distance from the source to the  $n^{th}$  receiver. The signals recorded by the cross dipole tool are therefore given by

$$xx_n(\omega) = g_f^{(n)}(\omega)s_x(\omega) \cos^2 \theta + g_s^{(n)}(\omega)s_x(\omega) \sin^2 \theta \quad (3)$$

$$xy_n(\omega) = [g_f^{(n)}(\omega)s_x(\omega) - g_s^{(n)}(\omega)s_x(\omega)] \cos \theta \sin \theta \quad (4)$$

$$yx_n(\omega) = [g_f^{(n)}(\omega)s_y(\omega) - g_s^{(n)}(\omega)s_y(\omega)] \cos \theta \sin \theta \quad (5)$$

$$yy_n(\omega) = g_f^{(n)}(\omega)s_y(\omega) \sin^2 \theta + g_s^{(n)}(\omega)s_y(\omega) \cos^2 \theta. \quad (6)$$

Assuming the same source function for both the x and y transducers,  $s_x(\omega) = s_y(\omega) = s(\omega)$ , and letting  $f_n(\omega) = g_f^{(n)}s(\omega)$  and  $s_n(\omega) = g_s^{(n)}s(\omega)$ , we can now represent equations 3 to 6 in matrix form

$$\begin{pmatrix} xx_n(\omega) & xy_n(\omega) \\ yx_n(\omega) & yy_n(\omega) \end{pmatrix} = \begin{pmatrix} \cos \theta & -\sin \theta \\ \sin \theta & \cos \theta \end{pmatrix} \begin{pmatrix} f_n(\omega) & 0 \\ 0 & s_n(\omega) \end{pmatrix} \times \begin{pmatrix} \cos \theta & \sin \theta \\ -\sin \theta & \cos \theta \end{pmatrix}. \quad (7)$$

## 2.1 Rotation

We can use equation 7 to create synthetic waveforms for a given source function and dispersion relations. Figures 2 and 3 show the difference between the borehole flexural mode recorded with a tool whose x and y axes are at an angle  $\theta = 25^\circ$  with the formation fast and slow axes, and the borehole flexural mode recorded with a tool which is aligned with the formation fast and slow axes. In matrix terms, if the tools

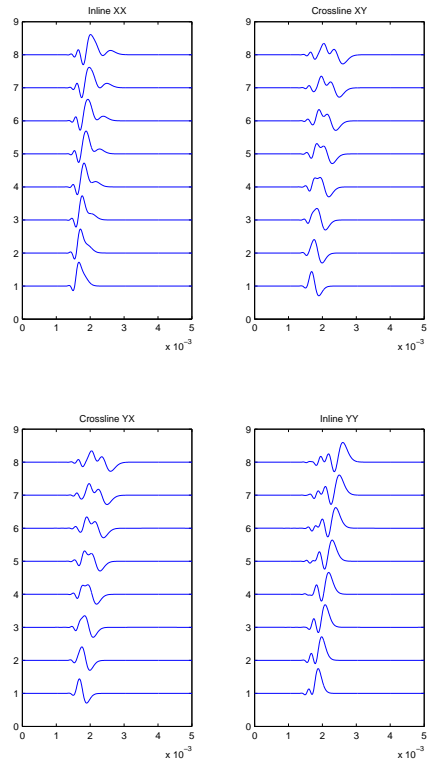


Figure 2: Time series representation of the borehole flexural mode with tool at angle  $\theta = 25^\circ$  with the formation axes.

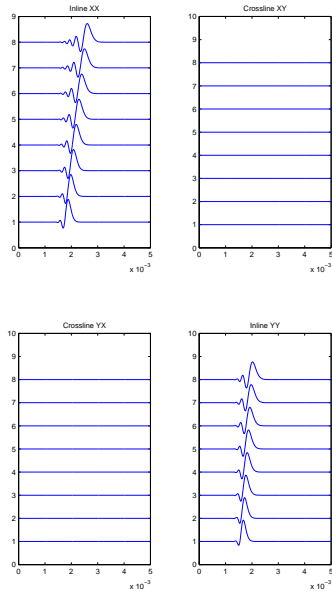


Figure 3: Time series representation of the borehole flexural mode with tool aligned ( $\theta = 90^\circ, 0^\circ$ ) with the formation axes .

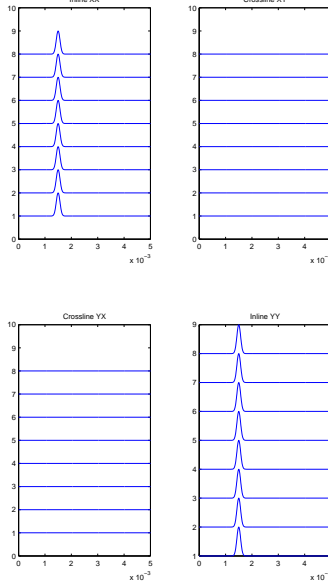


Figure 4: Time series representation of flexural mode after back propagation with the correct dispersion relation .

and formation axes are aligned, the diagonal components of equation 7 are maximized and the off diagonal components vanish.

We can invert 7

$$\begin{pmatrix} f_n(\omega) & 0 \\ 0 & s_n(\omega) \end{pmatrix} = \begin{pmatrix} \cos \theta & \sin \theta \\ -\sin \theta & \cos \theta \end{pmatrix} \begin{pmatrix} xx_n(\omega) & xy_n(\omega) \\ yx_n(\omega) & yy_n(\omega) \end{pmatrix} \times \begin{pmatrix} \cos \theta & -\sin \theta \\ \sin \theta & \cos \theta \end{pmatrix} \quad (8)$$

which gives the fast and slow propagation functions as,

$$f_n(\omega) = xx_n(\omega) \cos^2 \theta + [xy_n(\omega) + yx_n(\omega)] \sin \theta \cos \theta + YY_n(\omega) \sin^2 \theta \quad (9)$$

$$s_n(\omega) = xx_n(\omega) \sin^2 \theta - [xy_n(\omega) + yx_n(\omega)] \sin \theta \cos \theta + yy_n(\omega) \cos^2 \theta. \quad (10)$$

Additionally it is easy to see from equations 9 and 10 that if  $\theta = 90^\circ$  or  $0^\circ$  that there will be no  $xy_n(\omega)$  or  $yx_n(\omega)$  dependence.

## 2.2 Propagation

Next we undo the effects of propagation through the formation. Figure 4 shows the data from Figure 3 after the propagation has been undone. If the correct dispersion relation is used (i.e., each frequency component is back propagated at the right velocity), only the source function remains at each receiver on the inline arrays and since the correct rotation has been applied, there is no signal on the crossline arrays.

Remembering that  $f_n(\omega) = g_f^{(n)} s(\omega)$  and  $s_n(\omega) = g_s^{(n)} s(\omega)$ , we can write equation 8 as,

$$\begin{pmatrix} s(\omega) & 0 \\ 0 & s(\omega) \end{pmatrix} = \begin{pmatrix} e^{-i \frac{\omega}{v_f(\omega)} z_n} & 0 \\ 0 & e^{-i \frac{\omega}{v_s(\omega)} z_n} \end{pmatrix} \times \begin{pmatrix} \cos \theta & \sin \theta \\ -\sin \theta & \cos \theta \end{pmatrix} \begin{pmatrix} xx_n(\omega) & xy_n(\omega) \\ yx_n(\omega) & yy_n(\omega) \end{pmatrix} \begin{pmatrix} \cos \theta & -\sin \theta \\ \sin \theta & \cos \theta \end{pmatrix}. \quad (11)$$

Which is valid for any receiver  $n$ .

The propagation function has been moved to the righthand side. We now have a complete expression for the rotation and propagation of a source function to each of the array receivers. In other words, if the correct azimuthal angle and dispersion relations,  $v_f(\omega)$  and  $v_s(\omega)$ , are used in equation 11, we recover the source function  $s(\omega)$  at every receiver.

### 3 The Objective Function

In order to set up the inversion, we need to define an objective function whose minimum is the global best estimate of the parameters we are inverting for. In this case  $v_f(\omega)$ ,  $v_s(\omega)$  and  $\theta$ . The advantage of combining all the parameters in one objective function is that the inversion searches for the global minimum as opposed to a conditional result. Traditional processing first finds  $\theta$ , then inverts for velocity. This means that the best estimate for the velocity inversion is constrained by the  $\theta$  estimate, thus giving a conditional result.

We know that for the correct azimuth,  $\theta$ , the back rotated signals  $f_n(\omega)$  and  $s_n(\omega)$  will be maximized. We can therefore find the derivative of equations 9 and 10 and set it to zero (or minimize in the case of an inversion) to obtain the azimuthal angle,

$$\frac{\partial f_n(\omega)}{\partial \theta} = (yy_n - xx_n) \sin 2\theta + (xy_n + yx_n) \cos 2\theta = 0 \quad (12)$$

$$\frac{\partial s_m(\omega)}{\partial \theta} = (xx_m - yy_m) \sin 2\theta - (xy_m + yx_m) \cos 2\theta = 0 \quad (13)$$

where  $n$  and  $m$  refer to the receiver number for the fast and slow arrays, respectively. Since for the correct azimuth, both  $\frac{\partial f_n}{\partial \theta}(\omega)$  and  $\frac{\partial s_m}{\partial \theta}(\omega)$  would ideally be zero independently, their difference  $\frac{\partial f_n}{\partial \theta}(\omega) - \frac{\partial s_m}{\partial \theta}(\omega)$  also vanishes. However in order to have an objective function that is sensitive also to correlations in the data i.e., between receivers, we chose to minimize the quantity  $\int d\omega \left| \frac{\partial f_n}{\partial \theta}(\omega) - \frac{\partial s_m}{\partial \theta}(\omega) \right|^2$ . Note also that when the signal is incorrectly back-rotated, the  $f_n$  and  $s_n$  data both contain fast and slow components which are correlated and correctly picked-up by such an objective function

For the propagation, we know that if the correct velocity was used at each frequency, the data at each receiver will be back propagated to the source function. Thus if we undo the propagation correctly and subtract the signal from any receiver pair the absolute value of their difference should vanish.

Therefore our choice of objective function is ,

$$O[v_f(\omega), v_s(\omega), \theta] = \int_{\omega} \sum_{n,m} \left| \frac{\partial f_n(\omega)}{\partial \theta} - \frac{\partial s_m(\omega)}{\partial \theta} \right|^2 + |f_n(\omega) - s_m(\omega)|^2. \quad (14)$$

which is sensitive to both azimuth angle and fast and slow dispersion. Also, this objective function combines all the data from all receivers and it's minimization should therefore enable one to obtain the best fitting parameters (azimuth aswell as fast and slow mode dispersion curves) taking into account the maximum amount of information contained in the data. This is to be contrasted to more traditional methods (first estimate the azimuth independently of dispersion and then separately analyze the fast and slow mode data) that take only partial account of all the information contained in the data.

Ideally the inversion would search for the best velocity at each frequency as well as the optimal  $\theta$ . Unfortunately this would lead to a search space with  $2N+1$  parameters where  $N$  is the number of samples in frequency. Typically a cross-dipole tool has a source bandwidth of 5kHz and the number of unknown parameters would be in the order of 1000-10000. Since this is impractical, in terms of inversion, we parametrize the curves  $v_f$  and  $v_s$  as a polynomial reducing the inversion space to  $2(N+1)+1$  dimensions where  $N$  is now the order of polynomial. (Note a first order polynomial has two terms, thus for a straight line fit to the dispersion curve, the inversion has to search for 5 parameters.)

For purposes of this paper we used the Matlab function 'fminsearch.m' to perform the inversion. It uses a Multidimensional unconstrained nonlinear minimization (Nelder-Mead) algorithm. It was used merely for convenience and there is no reason why other non-linear inversion methods should not be successful. (least-squares, conjugate gradient or some monte-carlo based method).

To give some idea of the minimum of the objective function in the inversion space, Figures 5, 6 and 7 show results for data generated with  $v_f(\omega) = 4000\text{ms}^{-1}$  and  $v_s(\omega) = 2000\text{ms}^{-1}$  for all frequencies and  $\theta = 30^\circ$ . Using a constant value for the phase velocity as a function of frequency reduces the inversion search space to three, making it easy to visualize.

Using the correct value of  $2000\text{ms}^{-1}$  for the slow mode, Figure 5 shows the objective function space for the azimuthal angle against the fast mode velocity. The minimum can clearly be seen for  $v_f = 4000\text{ms}^{-1}$  and  $\theta = 30^\circ$ . Figure 6 shows the objective function space for  $v_s$  and  $\theta$  with the correct value for  $v_f = 4000\text{ms}^{-1}$ . Again the minimum is at the correct values of  $2000\text{ms}^{-1}$  for  $v_s$  and  $30^\circ$  for  $\theta$ . Similarly Figure 7 shows the minimum in function space for  $v_f$  and  $v_s$  with the correct value input for  $\theta$ .

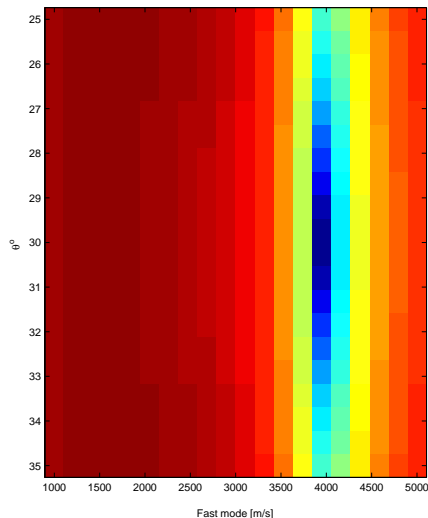


Figure 5: Magnitude of the objective function being minimized:  $\theta$  against  $v_f$  when the correct  $v_s$  is used. (red is high, blue is low)

## 4 Results with Synthetic Data

In this section we create a synthetic data set to test the inversion. To make the data we simulate a source using a simple Gaussian pulse as a function of time. We transform it to the frequency domain and propagate each frequency component to each receiver using a chosen dispersion relation for both the fast and slow modes. Figure 8 shows the source spectrum overlaid with the dispersion relationships. We have used a second order polynomial for the dispersion curves. It should be noted that the amplitude of the source is not significant. We now have the two principal flexural modes at each inline receiver as a function of frequency. We then use equations 3 to 6 to rotate the principal modes by some angle to get our cross-line components, and finally inverse Fourier transform the signal to get our data as a function of time. The data set used is the same as that in Figure 2, with an azimuthal angle  $\theta = 25^\circ$ .

The inversion successfully reproduces the dispersion relationship and finds the correct azimuth, as shown in Figure 9.

### 4.1 Synthetic Data with Noise

Next we added 10% white noise to the signal in the time domain and the inversion was run again. The inversion now estimates the azimuth to be  $22^\circ$ , which is  $3^\circ$  less than the true value of  $25^\circ$ . For the low frequencies the inversion matches very well with the true values. At high frequencies the match is not as good, but this is at the tail end of the source frequency spectrum thus there is not much frequency component to constrain the inversion. Figure 11 shows the noisy data after the rotation and back propagation given by

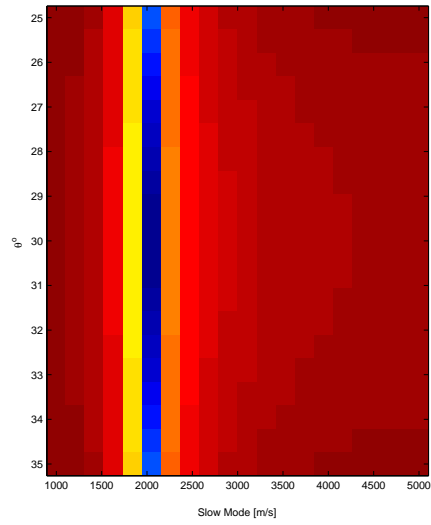


Figure 6: Magnitude of the objective function being minimized:  $\theta$  against  $v_s$  when the correct  $v_f$  is used. (red is high, blue is low)

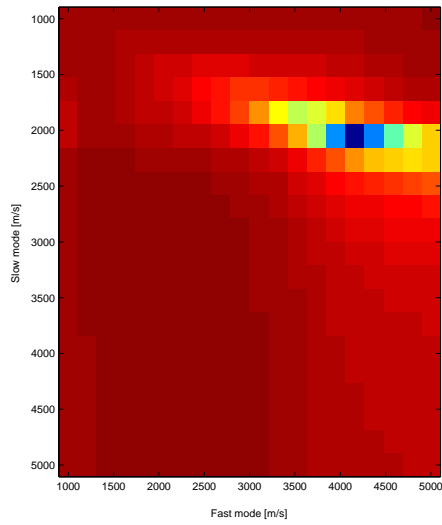


Figure 7: Magnitude of the objective function being minimized:  $v_s$  against  $v_f$  when the correct  $\theta$  is used. (red is high, blue is low)

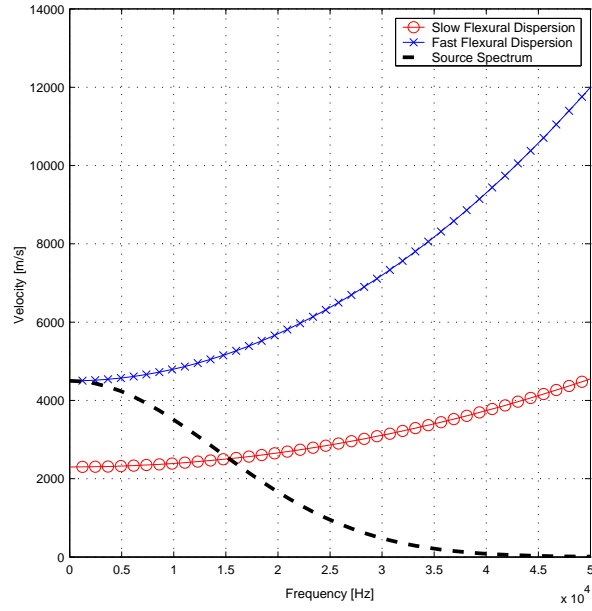


Figure 8: Source spectrum and dispersion relations for synthetic data.

the inversion. If the inversion has worked, this figure should look the same as Figure 4, i.e., each inline trace should look like the Gaussian source and the crossline traces should be zero. The effect of the noise remains but otherwise the results are as expected.

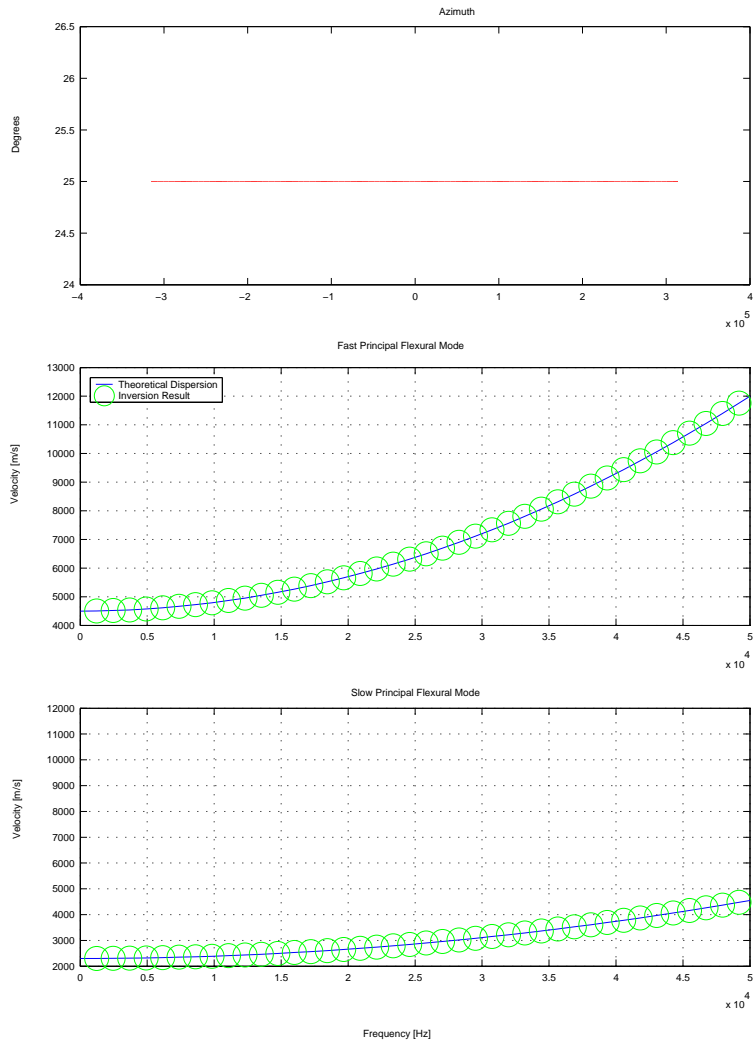


Figure 9: Inversion results.

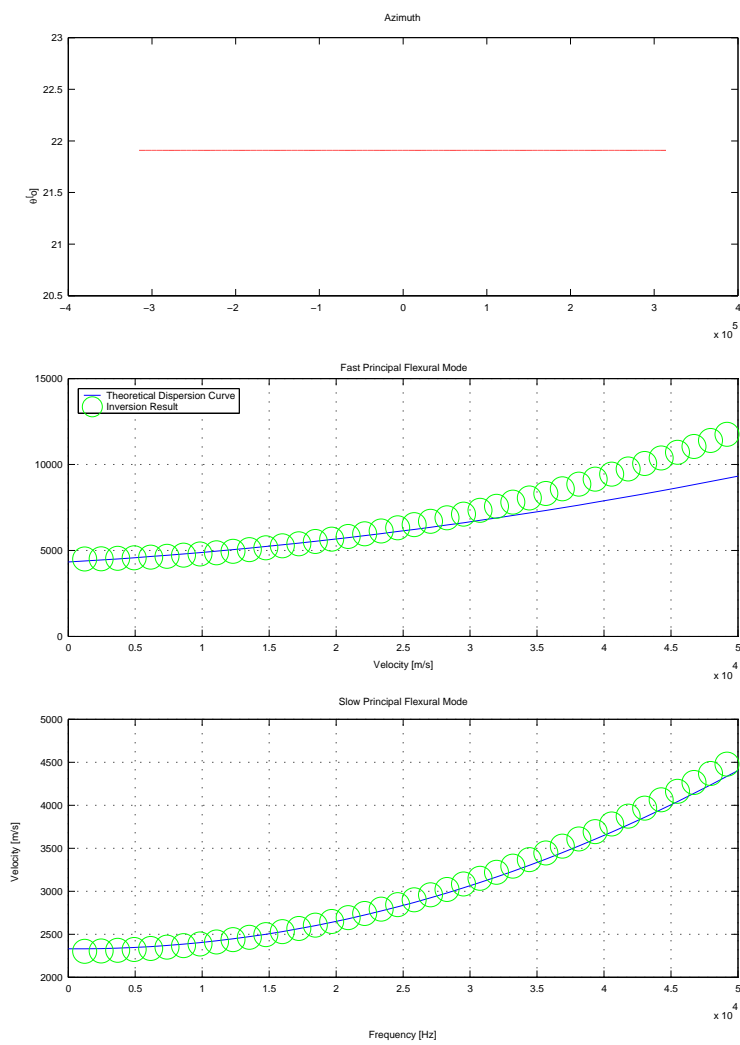


Figure 10: Inversion results for noisy data.

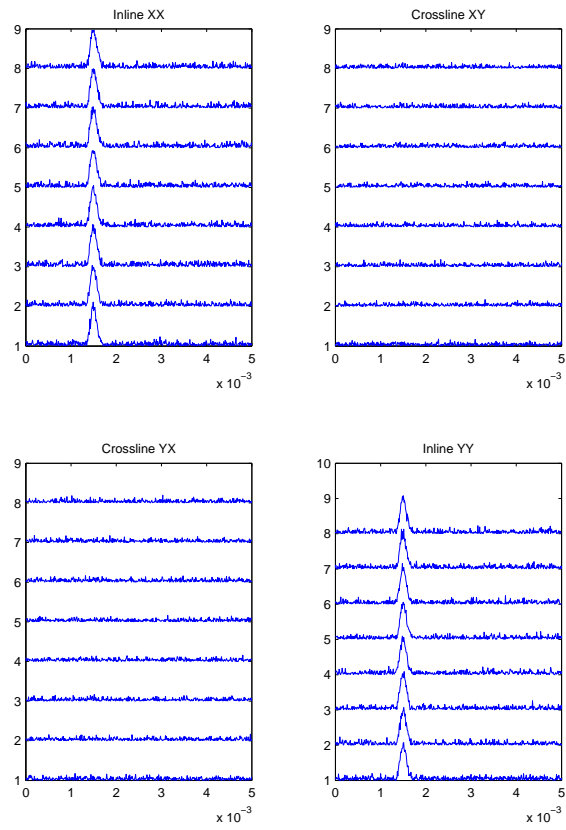


Figure 11: Noisy time series data after being rotated and back propagated with the output from the inversion.

## 5 Inversion of Borehole Data

In this section we use the inversion algorithm on some real cross-dipole data, Figure 12. The tool used to record the data was Schlumberger's Dipole Shear Sonic Imager (DSI). It contains 8 receiver pairs separated by 0.1524 m and two dipole sources with an offset of 3.35 m from the first receiver pairs. The source has a bandwidth of 80Hz to 5kHz. Figure 13 shows the spectrum of the recorded waveforms. The data is from an offshore well in Venezuela and the gamma ray from the same depth suggests a clean sand. Figure 14 shows the waveforms in semblance space. Semblance processing sweeps the data arrays at a fixed time for coherent energy arriving at a certain velocity, giving an image of phase velocity against time. It can be seen that there are arrivals in the data with phase speeds between 2000 and 3000 $ms^{-1}$ . Schlumberger's processing estimated the formation compressional velocity to be 4419 $ms^{-1}$  and shear velocity to be 2728 $ms^{-1}$ . Since we have used dipole data for the semblance processing we do not see the compressional arrival.

### 5.1 Processing and Results

Before inverting the waveforms for azimuth and dispersion relations, it is important to isolate the part of the waveform that represents the flexural mode. Since the borehole flexural mode consists of the lowest frequency components and propagates more slowly than the other generated waves, it may be isolated by time windowing and frequency bandpass filtering. Figure 15 shows a short fourier transform of the 1st and last receiver of the XX array. The short fourier transform allows us to identify frequency components arriving at a particular time. The black box on the plots indicates the part of the wave form that was used for the purpose of inversion. The results from the inversion can be seen in Figure 16. The formation exhibits weak anisotropy with the fast and slow flexural modes differing by less than 200 $ms^{-1}$ . Although the borehole flexural mode is highly dispersive in the right frequency interval, it does not change significantly over the frequencies sampled in the data. The inversion results agree very well with the semblance processing of the data, both flexural mode phase speeds fall in the coherent region on the semblance plot. In addition the inversion results show slight anisotropy which is not apparent from the semblance alone.

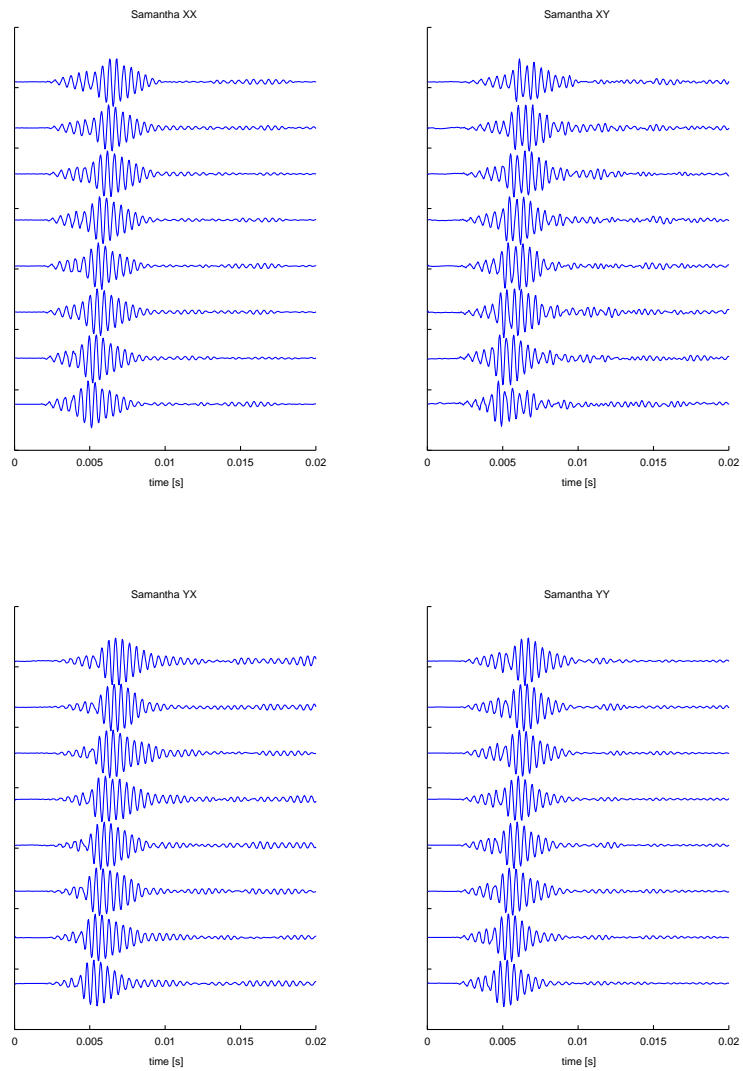


Figure 12: Cross dipole Data recorded by DSI tool in an offshore well in Venezuela.

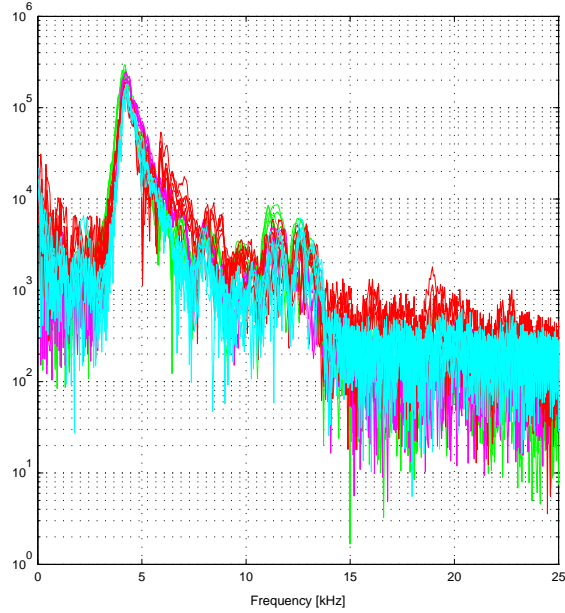


Figure 13: Frequency spectrum of Venezuela data.

## 6 Conclusions and Further Work

We have presented a new method for inverting borehole flexural waveforms, in anisotropic formations, for azimuth and frequency dependent phase velocities. The inversion allows a traditional multi-step processing to be condensed into a one-step inversion thus allowing a global best solution to be found.

The algorithm was shown to successfully invert synthetic data for the exact starting parameters used to form the data set. Results for noisy data also gave very good agreement. The process was also applied to field data and agreed well with traditional processing methods. The results show a weak anisotropy that was missed by processing the waveforms individually. Further work needs to be done to optimize the starting guess for the inversion procedure as the computation time is directly correlated to the ‘goodness’ of the starting guess. In this paper we used a polynomial parametrization for the fast and slow dispersion curves, further work can be done to find better representations as this too directly influences the computation time. It would also be interesting to examine the possibility of a multi-mode inversion as this would remove the need to filter the flexural mode from the waveforms which is not always a trivial step.

## 7 Acknowledgments

This work was supported by the Borehole Acoustics and Logging Consortium at the Massachusetts Institute of Technology.

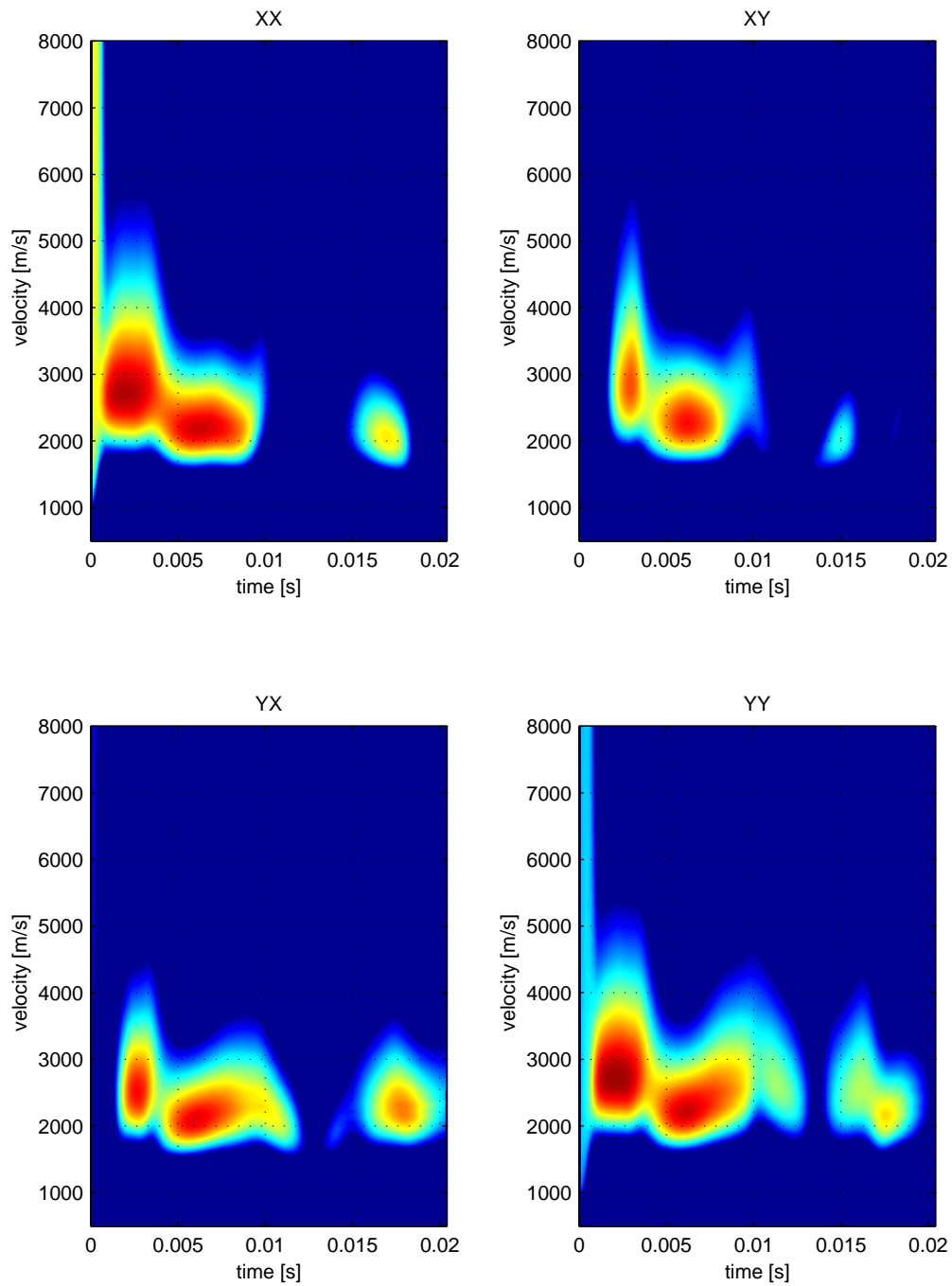


Figure 14: Semblance processing results of Venezuela data.

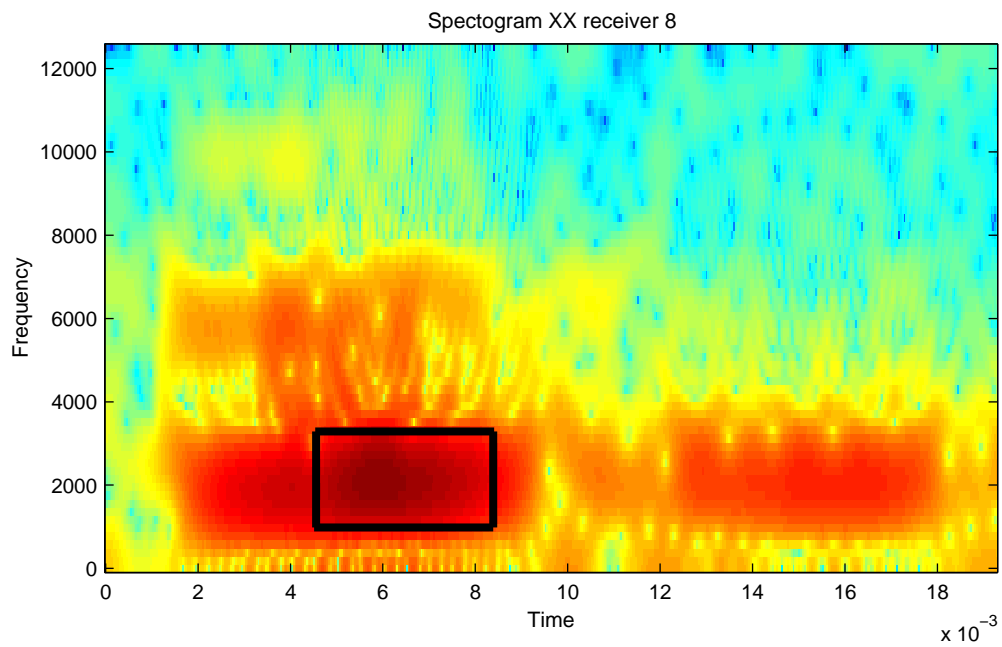
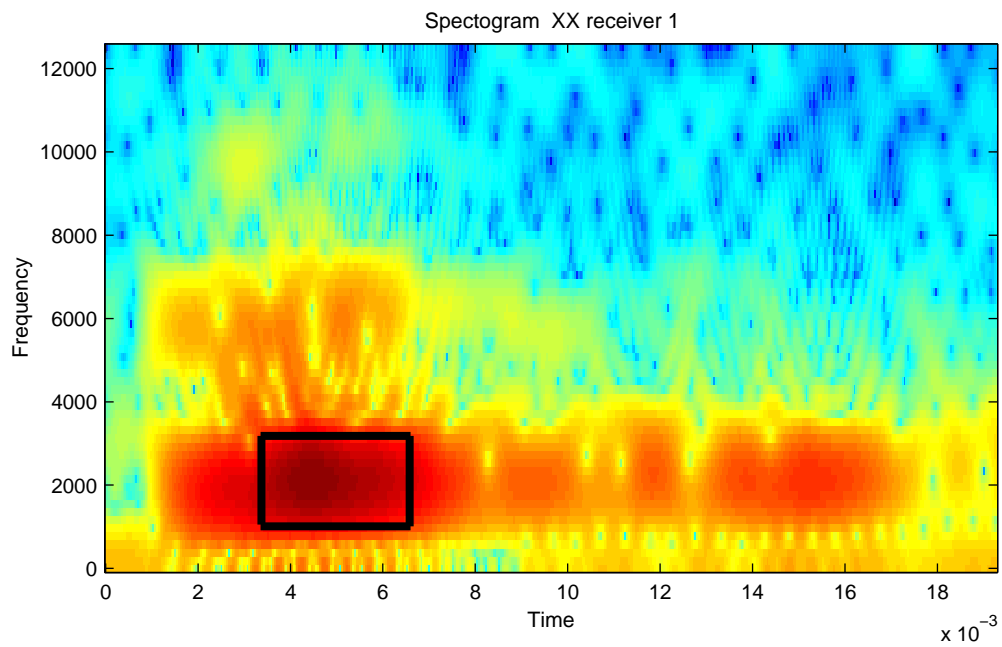


Figure 15: Spectrogram of the 1st and last waveforms from the XX array (Venezuela data).

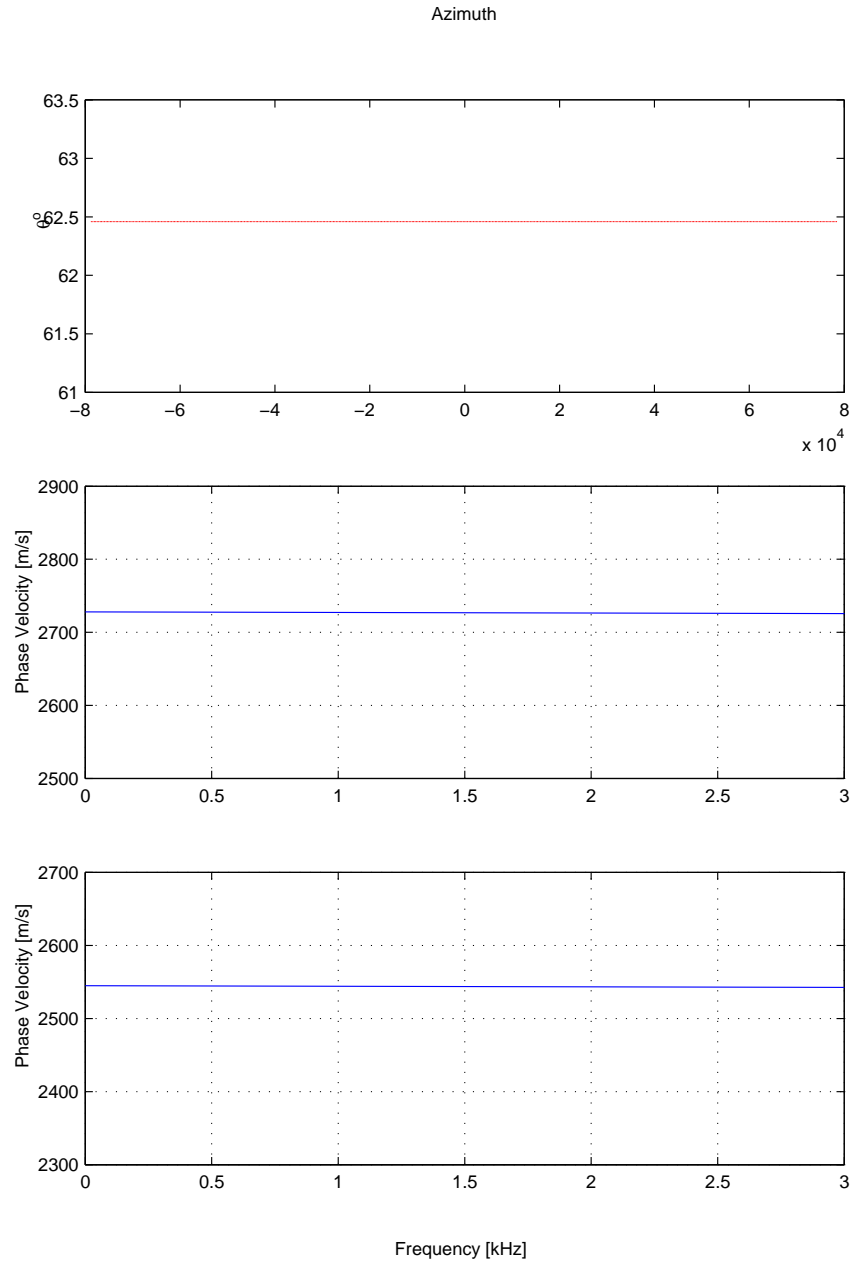


Figure 16: Inversion results when using a 2nd order polynomial to fit dispersion curves (Venezuela data).

## 8 References

Alford, R.M., 1986, Shear data in the presence of azimuthal anisotropy, *56th Ann. Int. Mtg., Soc. Expl. Geophys., Expanded Abstracts* 476-479.

Huang, X., 1999, A study of tectonic stresses in the Earth using standard acoustic logging, *Generals Exam Paper, E.A.P.S. M.I.T.*

Joyce, R. and Patterson, D., 1998 Advanced interpretation of fractured carbonate reservoirs using four-component cross-dipole analysis, *39th Ann. Mtg., Soc. Prof. Well Log Anal., Paper R.*

Tang, X. and Chunduru, R., 1999, Simultaneous inversion of formation shear-wave anisotropy parameters from cross-dipole acoustic-array waveform data, *Geophysics*, *64* 1502-1511.